WO_3/CeO_2 Nanocomposite Powders: Synthesis, Characterization, and Reactivity

Marta M. Natile,* Francesco Tomaello, and Antonella Glisenti

Dipartimento di Scienze Chimiche, Università di Padova, via F. Marzolo, 1-35131 Padova, Italy

Received February 14, 2006. Revised Manuscript Received May 5, 2006

WO_3/CeO_2 nanocomposite powders, characterized by increasing W/Ce atomic ratio, were prepared by depositing, by wet impregnation, different amounts of WO_3 on the CeO_2 surface. The powders were characterized by means of X-ray photoelectron and diffuse reflectance infrared Fourier transform spectroscopic techniques as well as thermal analysis. The WO_3/CeO_2 samples are slightly reduced with respect to the pure oxides: the presence of W(V) and Ce(III), in addition to W(VI) and Ce(IV), is evident at the interface supported/supporting oxides. Interesting information concerning particle dimensions and growth mode derive by X-ray diffraction and transmission electron microscopy. New acidic/basic and redox sites are evident on the surface of the WO_3/CeO_2 nanocomposites. The interaction with methanol was also investigated. Methanol interacts both molecularly and dissociatively with the WO_3/CeO_2 surface; the dissociation is prevalent on the sample characterized by a lower content of WO_3, whereas a mainly molecular interaction is observed with increasing amount of tungsten oxide. Oxidation of methanol is evident from $T \geq 423$ K on the sample with $[W/Ce]_{nominal} = 0.025$ and from $T \geq 473$ K on the one richer in WO_3. The reactivity toward methanol oxidation is higher in the sample with a lower content of WO_3, but the sample richer in WO_3 shows a higher selectivity with respect to formation of carbon dioxide.

Introduction

Interest in fuel cells has increased significantly in recent years. One of the main factors influencing their development is the worldwide concern about the consequences of fossil fuel use on the environment and public health.[1,2] Thanks to their higher efficiencies, fuel cells contribute to the reduction of emissions.[2] In this respect, the solid oxide fuel cell (SOFC) is one of the most promising designs because of the higher stability of the oxide materials. SOFCs have no problems with water management, flooding of the catalyst layer, or slow oxygen reduction kinetics. Moreover, internal reforming is possible in the SOFC over the anode catalyst.[3]

The anode in conventional designs is a composite of Ni and yttria-stabilized zirconia (YSZ) or Ni and a YSZ−CeO_2 solid solution.[3,4] Our interest is in development of novel nanocomposite oxide-based systems to be used as advanced anodes for intermediate temperature SOFC.

In this respect, nanocomposite oxide-based systems obtained depositing nanoparticles of an active oxide on a supporting one that is also an active catalyst offer great possibilities. In fact, beyond the huge reactivity of the supported nanoclusters,[5] if the overlayer does not completely wet the substrate, it is also possible to take advantage of the reactivity of the supporting oxide.

In this context the synthesis and characterization of WO_3/CeO_2 nanocomposite powders are considered. These systems were obtained by depositing (by wet impregnation) WO_3 clusters on the CeO_2 surface. Cerium oxide is a mixed conductor exhibiting both ionic (oxygen) and electronic conductivity (n-type); moreover, the oxygen storage capacity (OSC), associated with the ability of cerium to move between Ce(IV) and Ce(III), enhances its catalytic activity.[6] WO_3 is known to be a very active catalyst for oxidation reactions,[7−9] whereas the substoichiometric oxides ($WO_{2.95}$, $WO_{2.90}$, $WO_{2.75}$) show higher selectivity due to the presence of W(V) and/or W(IV) ions and crystallographic shear planes.[7,8]

The nanocomposite oxides were characterized with X-ray diffraction (XRD), thermal analysis (TGA), as well as X-ray photoelectron (XP) and diffuse reflectance infrared Fourier transform (DRIFT) spectroscopic techniques. The growing mechanism of the WO_3 clusters on the CeO_2 surface was investigated by means of transmission electron microscopy (TEM) and energy dispersive spectroscopy.

Particular attention is turned to characterization of the surface active sites and study of surface reactivity.

Investigation of active sites is fundamental for advanced catalysts design; acidic/basic sites, in fact, strongly influence the interaction between the catalyst surface and the reagents or the products, whereas to obtain oxidation products (to catalyze methanol oxidation for example) redox sites are

* To whom correspondence should be addressed. Phone: ++39-049-8275196. Fax: ++39-049-8275161. E-mail: martamaria.natile@unipd.it.

(1) Carrette, L.; Friedrich, K. A.; Stimming, U. *ChemPhysChem* **2000**, *1*, 162.
(2) Larmine, J.; Dicks, A. *Fuel Cell Systems Explained*; Wiley: New York, 2000.
(3) Minh, N. Q.; Takahashi, T. *Science and Technology of Ceramic Fuel Cells*; Elsevier: New York, 1995.
(4) Nakagawa, N.; Sagara, H.; Kato, K. *J. Power Sources* **2001**, *92*, 88.
(5) Klabunde, K. *Nanoscale Materials in Chemistry*; Wiley-Interscience: New York, 2001.
(6) Trovarelli, A. *Catal. Rev. Sci. Eng.* **1996**, *38*, 439.
(7) De Rossi, S.; Iguchi, E.; Schiavello, M.; Tilley, R. J. D. Z. *Phys. Chem. Neue Folge* **1976**, *103*, 193.
(8) Schiavello, M.; Pepe, F.; Cannizzaro, M.; De Rossi, A.; Tilley, R. D. Z. *Phys. Chem. Neue Folge* **1977**, *106*, 45.
(9) Haber, J.; Janas, J.; Schiavello, M.; Tilley, R. J. D. *J. Catal.* **1983**, *82*, 395.

10.1021/cm0603654 CCC: $33.50
Published on Web 06/09/2006

necessary. In this regard the active sites distributed on the catalyst surfaces were investigated by means of probe molecules (pyridine and carbon monoxide are usually used for acidic sites, while carbon dioxide is used for basic sites;[10−18] carbon monoxide is also used to test redox sites), and the results were compared with those obtained on CeO_2[19] and WO_3.[20]

The surface reactivity of the nanocomposite samples toward methanol was considered. Methanol is both an important probe molecule and an interesting combustible for fuel cells.[2]

It is worth underlining that the study of the active sites and reactivity was carried out on the samples as prepared, avoiding any activation or cleaning treatment.

Experimental Session

(a) Catalyst Preparation. The CeO_2 support was prepared by precipitation from a basic solution of $Ce(NO_3)_3 \cdot 6H_2O$ (Strem Chemicals 99.9%). The solution was obtained by dissolving nitrate in distilled water and adding, under vigorous stirring, NH_3 (AnalaR 25%) until pH = 10. The precipitate was filtered out and washed with distilled water until pH = 7; then it was dried at 373 K for 5 h and calcined at 523 K for 5 h (in air). The supporting powder was investigated by means of XRD, XP, and DRIFT spectroscopic techniques and thermal analysis and confirmed to be CeO_2 before the deposition procedure.[19] The WO_3/CeO_2 nanocomposite systems were obtained by wet impregnation of CeO_2 (calcined at 523 K) with aqueous solutions containing increasing quantities of ammonium metatungstate, $(NH_4)_6(W_{12}O_{39}) \cdot H_2O$ (Aldrich): $[W/Ce]_{nominal}$ = 0.010, 0.025, 0.040, 0.055, 0.070, 0.085 (nominal atomic ratios are obtained from the precursors weighed quantities). The obtained suspension was maintained under stirring for 2 days and then kept at rest for 1 day. Water was evaporated in air, and the obtained solid was dried at 373 K for 5 h and calcined at 773 K for 5 h (in air). The WO_3 powder used as the reference was prepared by heat treatment of the tungstic acid precipitated from an acid solution of $(NH_4)_6(W_{12}O_{39}) \cdot H_2O$. The precipitated tungstic acid was filtered out and rapidly washed with distilled water until pH = 7; then it was dried at 373 K in air for 1 h and calcined at 773 K for 24 h (in air).

(b) XPS Measurements. XPS spectra were recorded using a Perkin-Elmer PHI 5600 ci spectrometer with a standard Al Kα source (1486.6 eV) working at 350 W. The working pressure was less than 7×10^{-7} Pa. The spectrometer was calibrated by assuming the binding energy (BE) of the Au $4f_{7/2}$ line to lie at 84.0 eV with respect to the Fermi level. Extended spectra (survey) were collected in the range 0−1350 eV (187.85 eV pass energy, 0.4 eV step, 0.05 s $step^{-1}$). Detailed spectra were recorded for the following regions: Ce 3d, Ce 4d, W 4f, W 4d, O 1s, and C 1s (11.75 eV pass energy, 0.1 eV step, 0.1 s $step^{-1}$). The standard deviation in the BE values of the XPS line is 0.10 eV. The atomic percentage, after a Shirley-type background subtraction,[21] was evaluated using the PHI sensitivity factors.[22] To take into consideration charging problems the C 1s peak at 285.0 eV was considered and the peak BE differences were evaluated. The sample for the XPS analysis was processed as a pellet by pressing the catalyst powder at ca. 6×10^7 Pa for 10 min; the pellet was then evacuated for 12 h at ca. 1×10^{-3} Pa.

(c) DRIFT Measurements and Reaction Conditions. The IR spectra were collected in a Bruker IFS 66 spectrometer (accumulating 128 scans at a resolution of 4 cm^{-1}) and displayed in the Kubelka−Munk units.[23,24] The temperature of the powder was checked by means of a thermocouple inserted into the sample holder directly in contact with the powder.

Prior to each experiment, ca. 10 mg of the sample was loaded in the high-temperature high-pressure (HTHP) cell installed in the COLLECTOR apparatus for diffuse reflectance infrared Fourier transform (DRIFT) spectroscopy from Spectra-Tech, Inc. fitted with ZnSe windows. Before measurement, the powder was kept in nitrogen flow to eliminate water traces until a stable IR spectrum was obtained (ca. 2 h). Then the sample was exposed to the reactive species for 2 min at a flow rate of ca. 100 cm^3 min^{-1}. The background spectrum of the clean surface was measured for spectra correction. The HTHP chamber was filled with the pyridine or alcohol vapors, flowing nitrogen through a bubbler containing the liquid, whereas for CO (Air Liquide, 99.997%) and CO_2 (Air Liquide, 99.998%) the gas outlet was directly connected to the reaction chamber. Pyridine and methanol used for the chemisorption were taken from a commercial source (Sigma-Aldrich, spectroscopic grade) and used without further purification.

(d) Thermal Analysis and XRD. Thermogravimetric analysis (TGA) was carried out in a controlled atmosphere using the Simultaneous Differential Techniques (SDT) 2960 of TA Instruments. Thermograms were recorded at 5 K min^{-1} heating rates in air and nitrogen flow. The temperature ranged from room temperature (RT) to 1273 K.

XRD patterns were obtained with a Bruker "D8 Advance" diffractometer with Bragg−Brentano geometry using Cu Kα radiation (40 kV, 40 mA, $\lambda = 0.154$ nm).

(e) TEM and EDS. Transmission electron micrographs were obtained with a Philips JRM 2010 electron microscope using 200 kV primary voltage. The samples used for TEM observations were prepared by dispersing some products in ethanol followed by ultrasonic vibration for 30 min and then placing a drop of the dispersion onto a copper grid (200 Cu) coated with a layer of amorphous carbon. Energy dispersive spectroscopy (EDS) measurements were carried out by means of a LINK INCA 100 microanalysis system. The diameter of the analyzed spot was 5−15 nm.

Results and Discussion

(a) WO_3/CeO_2 Characterization. The XP spectra obtained for the powder oxides are shown in Figures1 and 2, whereas the peak positions are summarized in Table 1. It is important to underline that the minimum exposure time (determined by repeated measures at increasing irradiation time) was used to avoid ceria reduction under XPS condi-

(10) Parry, E. P. *J. Catal.* **1963**, *2*, 371.
(11) Little L. H. *Infrared Spectra of Adsorbed Species*; Academic Press: San Diego, CA, 1966; Chapter 7.
(12) Nortier, P.; Fourre, P.; Mohammed Saad, A. B.; Saur, O.; Lavalley, J. C. *Appl. Catal.* **1990**, *61*, 141.
(13) Busca, G. *Catal. Today* **1998**, *41*, 191.
(14) Auroux, A.; Gervasini, A. *J. Phys. Chem.* **1990**, *94*, 6371.
(15) Rethwisch, D. G.; Dumesic, J. A. *Langmuir* **1986**, *2*, 73.
(16) Lavalley, J. C. *Trends Phys. Chem.* **1991**, *2*, 305.
(17) Martin, D.; Duprez, D. *J. Mol. Catal. A: Chem.* **1997**, *118*, 113.
(18) Vannice, M. H. In *Catalysis Science and Technology*; Anderson, J. R., Boudart, M., Eds.; Springer-Verlag: New York, 1982; Vol. 3, Chapter 3.
(19) Natile, M. M.; Boccaletti, G.; Glisenti, A. *Chem. Mater.* **2005**, *17*, 6272.
(20) Natile, M. M.; Glisenti, A. Unpublished data.
(21) Shirley, D. A. *Phys. Rev.* **1972**, *55*, 4709.
(22) Moulder, J. F.; Stickle, W. F.; Sobol, P. E.; Bomben, K. D. In *Handbook of X-ray Photoelectron Spectroscopy*; Chastain, J., Ed.; Physical Electronics: Eden Prairie, MN, 1992.
(23) Kubelka, P.; Munk, F. *Z. Tech. Phys.* **1931**, *12*, 593.
(24) Kortum, G. *Reflectance Spectroscopy*; Springer: New York, 1969.

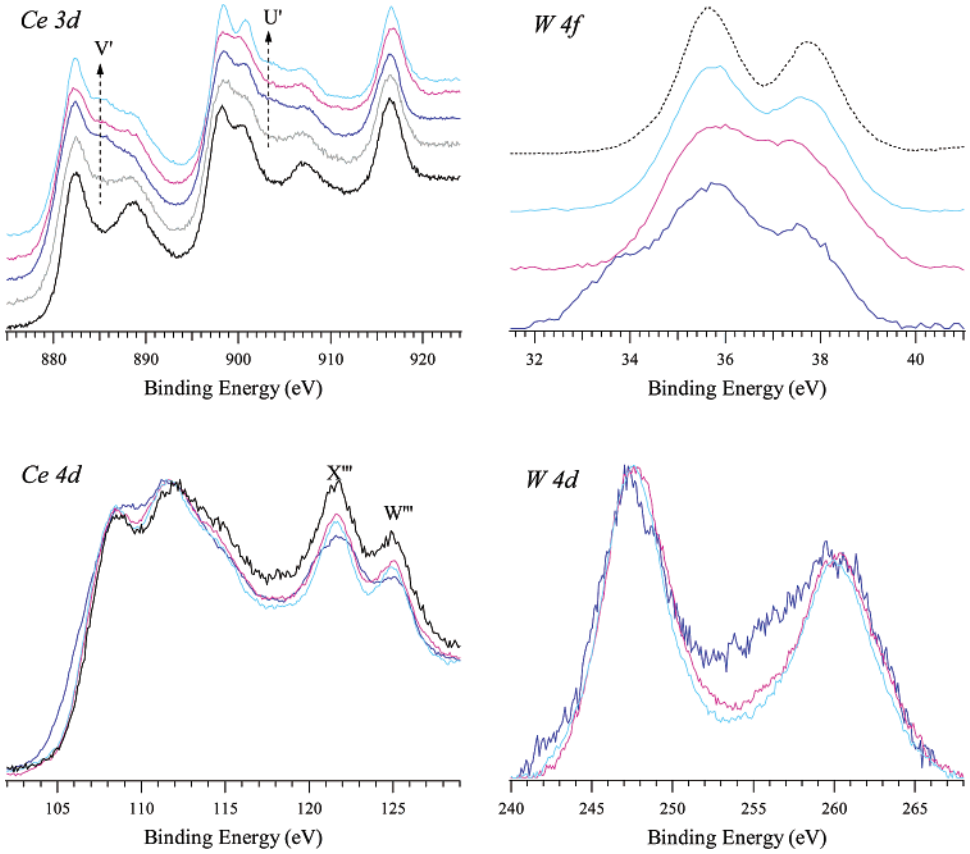

Figure 1. Ce 3d, Ce 4d, W 4f, and W 4d XP spectra obtained on the WO_3/CeO_2-supported oxides compared with the corresponding spectra of pure oxides: (black line) CeO_2 treated at 523 K, (gray line) CeO_2 treated at 773 K, (dotted line) WO_3 treated at 773 K, $[W/Ce]_{nominal}$ = (blue line) 0.025, (magenta line) 0.070, (turquoise line) 0.085. (The spectra are normalized with respect to their maximum value.)

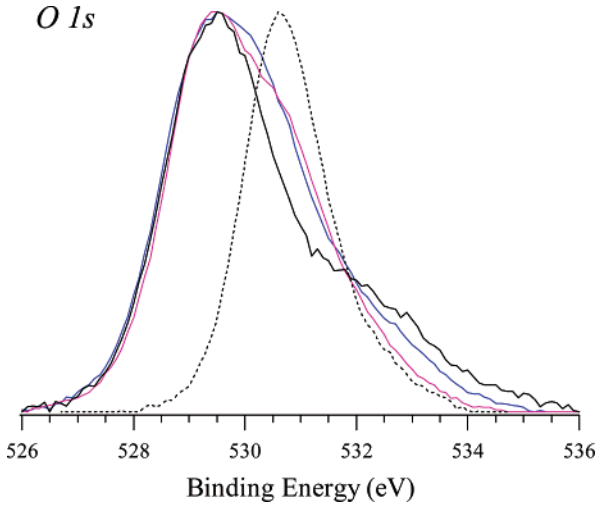

Figure 2. O 1s XP spectra obtained on the WO_3/CeO_2–supported oxides compared with the corresponding spectra of the pure oxides: (black line) CeO_2 treated at 523 K, (dotted line) WO_3 treated at 773 K, $[W/Ce]_{nominal}$ = (blue line) 0.025, (magenta line) 0.070. (The spectra are normalized with respect to their maximum value.)

tions, which is well documented in the literature.[25] Analysis of the Ce 3d peak positions and shape (Figure 1) and comparison with the values obtained for CeO_2 and with literature data (Table 1) suggest the presence of both Ce(IV) and Ce(III) cations on the surface (the signals characteristic of Ce(III), V′ and U′, are very evident in Figure 1).[19,26,27] Two factors can be responsible for the presence of Ce(III): treatment at high temperature and deposition of tungsten oxide. Comparison with the spectrum of CeO_2 treated at 773 K (i.e., the same temperature used for heat treatment of the WO_3/CeO_2 powders) confirms the contribution of the tungsten oxide deposition to the ceria reduction. Moreover, a detailed investigation of the Ce 4d region (Figure 1) reveals that the reduction phenomenon is not only in the outer layers:[33] the signals X‴ and W‴ characteristic of Ce(IV) are less evident in the WO_3/CeO_2 nanocomposites than in CeO_2.

The W 4f and W 4d peak positions observed in the different nanocomposite samples (Table 1 and Figure 1) agree with the expected values for W(VI) in WO_3 (Table 1). Comparison of the W 4f peaks of the pure and nanocomposite oxide samples (Figure 1) reveals, however, a different peak shape. A shoulder at the low BE side (~33.6 eV), particularly evident in samples characterized by $[W/Ce]_{nominal} \leq 0.025$, is consistent with the existence of W(V) at the interface between CeO_2 and WO_3.[34]

(25) Park, P. W.; Ledford, J. S. *Langmuir* **1996**, *12*, 1794.
(26) Mullins, D. R.; Overbury, S. H.; Huntley, D. R. *Surf. Sci.* **1998**, *409*, 307.
(27) Rama Rao, M. V.; Shripathi T. *J. Electron Spectrosc. Relat. Phenom.* **1997**, *87*, 121.
(28) Praline, G.; Koel B. E.; Hance, R. L.; Lee, H.-I.; White, J. M. *J. Electron Spectrosc. Relat. Phenom.* **1980**, *21*, 17.
(29) *Nist XPS Database 20*, Version 3.4 (Web Version):http://srdata.nist.gov/xps/.
(30) Salvati, L. Jr.; Makovsky, L. E.; Stencel, J. M.; Brown, F. R.; Hercules, D. M. *J. Phys. Chem.* **1981**, *85*, 3700.
(31) Tocchetto, A.; Glisenti, A. *Langmuir* **2000**, *16*, 6173.
(32) Khyzhun, O. Yu. *J. Alloys Compd.* **2000**, *305*, 1.
(33) Escape depth is higher for Ce 4d than Ce 3d photoelectrons. Seah, M. P.; Dench, W. A. *Surf. Interface Anal.* **1979**, *1*, 2.

Table 1. XPS Peak Positions (binding energy, eV) Obtained for the WO_3/CeO_2-Supported Oxide Samples and Pure Oxide (literature data also reported for comparison)

		Ce $3d_{5/2}$		Ce $3d_{3/2}$			
samples	O 1s	V	V′	U‴	W $4f_{7/2}$	W $4f_{5/2}$	W $4d_{5/2}$
W/Ce = 0.010	529.4	883.1	885.6	916.3	35.7	37.6	246.9
W/Ce = 0.025	529.5	882.4	885.7	916.5	35.7	37.5	246.9
W/Ce = 0.040	529.6	882.3	885.5	916.5	35.6	37.6	247.5
W/Ce = 0.055	529.5	882.4	885.4	916.7	35.7	37.6	247.4
W/Ce = 0.070	529.5	882.4	885.8	916.7	35.7	37.6	247.6
W/Ce = 0.085	529.7	882.5	885.8	916.6	35.6	37.7	247.6
CeO_2[19]	529.6	882.9		916.8			
CeO_2[25−28]	529.0−530.4	882.6		916.6−916.8			
Ce_2O_3[25,26,28]	530.7		885.4				
Ce[29]		883.2−883.9					
WO_3[a]	530.6				35.6	37.7	
WO_3[30−32]	530.3−530.8				35.3−35.5	37.6	247.8−248.2
H_2WO_4[29]	530.2−530.7				35.9−36.0		247.6
WO_2[29]	530.4−530.8				32.7−33.4		243.5
W[29]					30.9−31.6		243.5−244.0

[a] This work.

Table 2. Nominal and XPS Atomic Composition of the Supported Oxides

sample	$[W/Ce]_{nominal}$	$[W4f/Ce3d]_{XPS}$	$[W4d/Ce3d]_{XPS}$	$[O1s/(W4f+Ce3d)]_{XPS}$
1	0.010	0.02	0.03	1.56
2	0.025	0.03	0.05	1.64
3	0.040	0.05	0.09	1.60
4	0.055	0.07	0.12	1.61
5	0.070	0.08	0.14	1.80
6	0.085	0.10	0.18	1.72

The positions of the O 1s XP peak (Figure 2) in the WO_3/CeO_2 samples (529.4−529.7 eV) agree with the expected value for oxygen in ceria (Table 1).[19] The fitting procedure shows the presence of two contributions at higher BE: one of them, at 530.4 eV, can be attributed to Ce(III)−O[25−28] and W−O[31] and the other (532.0 eV) to the presence of hydroxyl groups.[35] The signal at 532.0 eV decreases with the W/Ce atomic ratio, thus indicating a lower surface hydroxylation in the samples richer in WO_3.

The XP atomic composition is reported as a function of the nominal one in Table 2. Consistent with the surface-specific character of the XP spectroscopy and the preparation procedure, the obtained W/Ce atomic ratios are always higher than the corresponding nominal values (calculated from the weighted quantities). The W 4f/Ce 3d atomic ratio is always lower than W 4d/Ce 3d; this means that WO_3 is segregated on the surface and no diffusion phenomena occur.[36] The O 1s/(W 4f + Ce 3d) atomic ratio is lower than the nominal value, confirming the poor surface hydroxylation. The surface reduction observed with decreasing WO_3 content also has to be considered.

Figure 3 shows the XRD patterns of a series of WO_3/CeO_2 samples with different WO_3 loadings. The XRD patterns of CeO_2 and WO_3 are also reported for comparison. The XRD patterns obtained for the WO_3/CeO_2 samples coincide with that of pure CeO_2; no diffraction peaks of crystalline WO_3 are observed. This suggests that WO_3 exists as highly dispersed or amorphous surface species or the tungsten oxide amount is low.[37,38] The average diameter of the WO_3/CeO_2 crystallites, evaluated by means of the Scherrer formula,[39] is about 13 nm, whereas for the supporting ceria the particle's average diameter is about 9 nm. This difference could be ascribed to the heat treatment at 773 K. The WO_3 contribution should not be excluded.

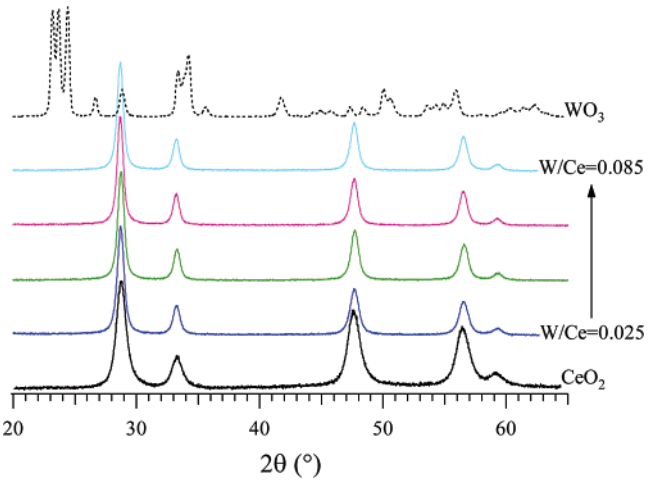

Figure 3. XRD patterns of the WO_3/CeO_2-supported oxides with $[W/Ce]_{nominal}$ = (blue line) 0.025, (green line) 0.040, (magenta line) 0.070, (turquoise line) 0.085 compared with the patterns obtained for CeO_2 treated at 523 K (black line) and WO_3 treated at 773 K (dotted line).

Two supported oxides characterized by atomic ratios $[W/Ce]_{nominal}$ = 0.025 and 0.070 were selected for more detailed investigation.

TEM images of WO_3/CeO_2 nanocomposite samples characterized by atomic ratios $[W/Ce]_{nominal}$ = 0.025 and 0.070 are shown in Figure 4. For both the samples the TEM images do not show the WO_3 particles distributed on the CeO_2 surface. The ED spectra, collected in different points of the samples, show the presence of tungsten. The EDS W/Ce atomic ratios agree with the values obtained by XPS (Table 3, compare with W 4f/Ce 3d atomic ratio). Moreover, the obtained values are rather similar in the different points, thus

(34) Chappel, P. J. C.; Kibel; M. H.; Baker, B. G. *J. Catal*. **1988**, *110*, 139.
(35) McIntyre, N. S.; Chan, T. C. In *Practical Surface Analysis 1*, 2nd ed.; Briggs, D., Seah, M. P., Eds.; Wiley: Chichester, U.K., 1990; Chapter 10.
(36) Escape depth is higher for W 4f than W 4d photoelectrons. See also ref. 33.
(37) Bigey, C.; Hilaire, L.; Maire, G. *J. Catal*. **2001**, *198*, 208.
(38) Klug, H. P.; Alexander, L. E. *X-ray Diffraction Procedures* − For Polycrystalline and Amorphous Materials, 2nd ed.; Wiley: New York, 1974; Chapter 9.
(39) Enzo, S.; Polizzi, S.; Benedetti, A. *Z. Krystall*. **1985**, *170*, 275.

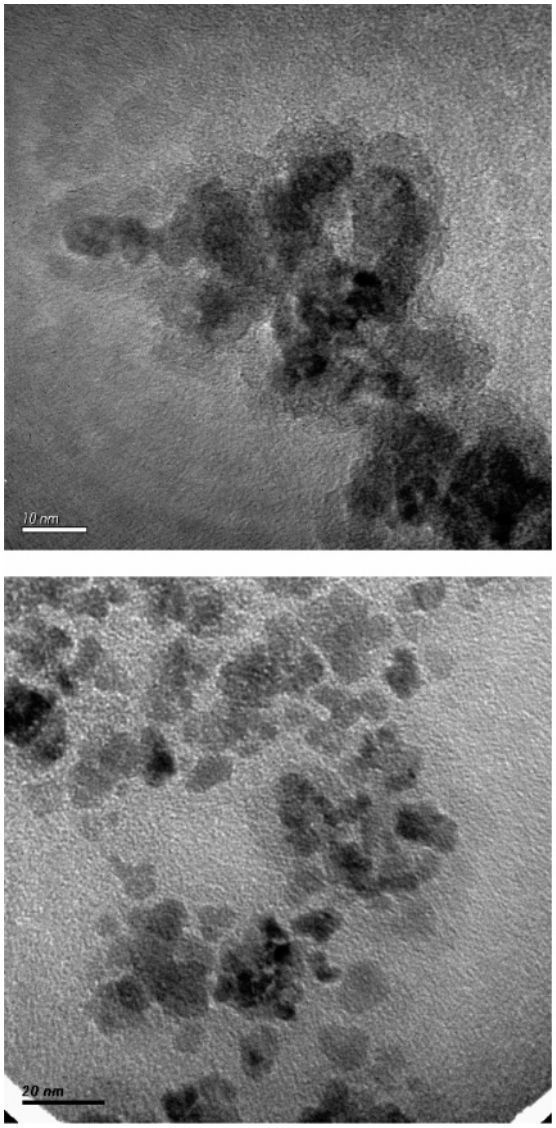

Figure 4. TEM images of the WO_3/CeO_2-supported oxides. (A) Sample with $[W/Ce]_{nominal} = 0.025$. (B) Sample with $[W/Ce]_{nominal} = 0.070$.

Table 3. EDS Atomic Ratios Obtained in Different Regions of the Supported Oxides with $[W/Ce]_{nominal} = 0.025$ and 0.070

region W/Ce = 0.025	W/Ce	region W/Ce = 0.070	W/Ce
1	0.035	1	0.066
2	0.034	2	0.082
3	0.024	3	0.069
4	0.030	4	0.076
5	0.029	5	0.071
6	0.027	6	0.074
7	0.051	7	0.053
8	0.038	8	0.100
9	0.031	9	0.075
10	0.046	10	0.078

suggesting a homogeneous distribution of WO_3 on the supporting surface. TEM and EDS outcomes suggest a Frank-van der Merwe growth mechanism.[40] A different growing mechanism was observed for the CoO_x/CeO_2 nanocomposite powders: at low cobalt content 2D cobalt oxide clusters grow on the CeO_2 supporting surface, whereas with increasing cobalt content the supported oxide is homogeneously distributed on the support surface.[41] In agreement with the results obtained by means of the Scherrer formula, the average dimensions of the WO_3/CeO_2 nanocomposite oxide particles determined from the TEM images are around 12 nm.

The DRIFT spectra obtained for the nanocomposite oxides with $[W/Ce]_{nominal} = 0.025$ and 0.070 are reported, as a function of temperature, in Figure 5. In the spectral region of the O−H stretching vibrations (Figure 5a,c) several signals are evident at 3215, 3410, 3511, 3654, and 3680 cm^{-1}. These contributions are attributed to molecularly chemisorbed water (3215 cm^{-1}), whose presence is confirmed by the OH bending at 1628 cm^{-1}, H-bound hydroxyl groups (3410 cm^{-1}), and OH groups tri- and bicoordinated (3511 and 3654 cm^{-1}, respectively) to Ce(IV) cations.[42] The peak at 3680 cm^{-1} can be due to OH groups bicoordinated to Ce(IV) and Ce(III).[42]

It is worth noting that the hydroxyl groups revealed in WO_3 (3596, 3627, 3690−3700, and 3730 cm^{-1})[31] are not evident.

Heat treatment causes desorption of molecularly chemisorbed water molecules as well as condensation of the H-bound OH groups: the signals corresponding to these species are no longer visible at $T > 373$ K. The intensity of the peaks attributed to the stretching vibration of bi- and tricoordinated hydroxyl groups also decreases with temperature; their shift toward lower wavenumbers suggests a hydroxyl lateral interaction.[43] These signals are still evident at 523 K in the sample with $[W/Ce]_{nominal} = 0.025$ (Figure 5a) and at 623 K in the sample with $[W/Ce]_{nominal} = 0.070$ (Figure 5c).

The obtained results agree with the thermal analysis ones. Thermal analysis was carried out in both nitrogen and air flow without significant differences. The thermal spectra indicate water desorption at $T < 400$ K followed by a quite low and continuous weight loss due to condensation of H-bound hydroxyl groups (Figure 6). However, weight loss due to decomposition of carbonate species cannot be excluded as suggested by the DRIFT outcomes. It is also evident that the weight loss is lower in the sample characterized by a higher W/Ce atomic ratio. Consistently, the weight loss in WO_3 is very low. Concerning the supporting ceria, the weight decrease, in contrast, is more significant from room temperature to about 850 K, thus indicating the presence of water tightly bonded to the oxide surface and condensation of hydroxyl groups.[19]

The lower hydroxylation of the nanocomposite samples with respect to CeO_2 could indicate grafting of WO_3 to CeO_2 by condensation of OH groups.[44]

In the IR spectral region characteristic of the O−C−O stretching vibrations several signals can be observed (Figure 5b,d). The peaks revealed in the nanocomposite oxide with $[W/Ce]_{nominal} = 0.025$ are centered at 1298, 1475, 1506, and 1541 cm^{-1}. Comparison with literature data suggests the presence of mono- (1475 cm^{-1})[45] and bidentate (1298 and

(40) Argile, C.; Rhead, G. E. *Surf. Sci. Rep.* **1989**, *10*, 277.
(41) Natile, M. M.; Glisenti, A. *Chem. Mater.* **2005**, *17*, 3403.
(42) Badri, A.; Binet C.; Lavalley, J.-C. *J. Chem. Soc., Faraday Trans.* **1996**, *92*, 4669.
(43) Zecchina, A.; Lamberti, C.; Bordiga, S. *Catal. Today* **1998**, *41*, 169.
(44) Schwarz, J. A.; Contescu, C.; Contescu, A. *Chem. Rev.* **1995**, *95*, 477.
(45) Li, C.; Sakata Y.; Arai, T.; Domen, K.; Maruya, K.-I.; Onishi, T. *J. Chem. Soc., Faraday Trans. 1* **1989**, *85*, 929.

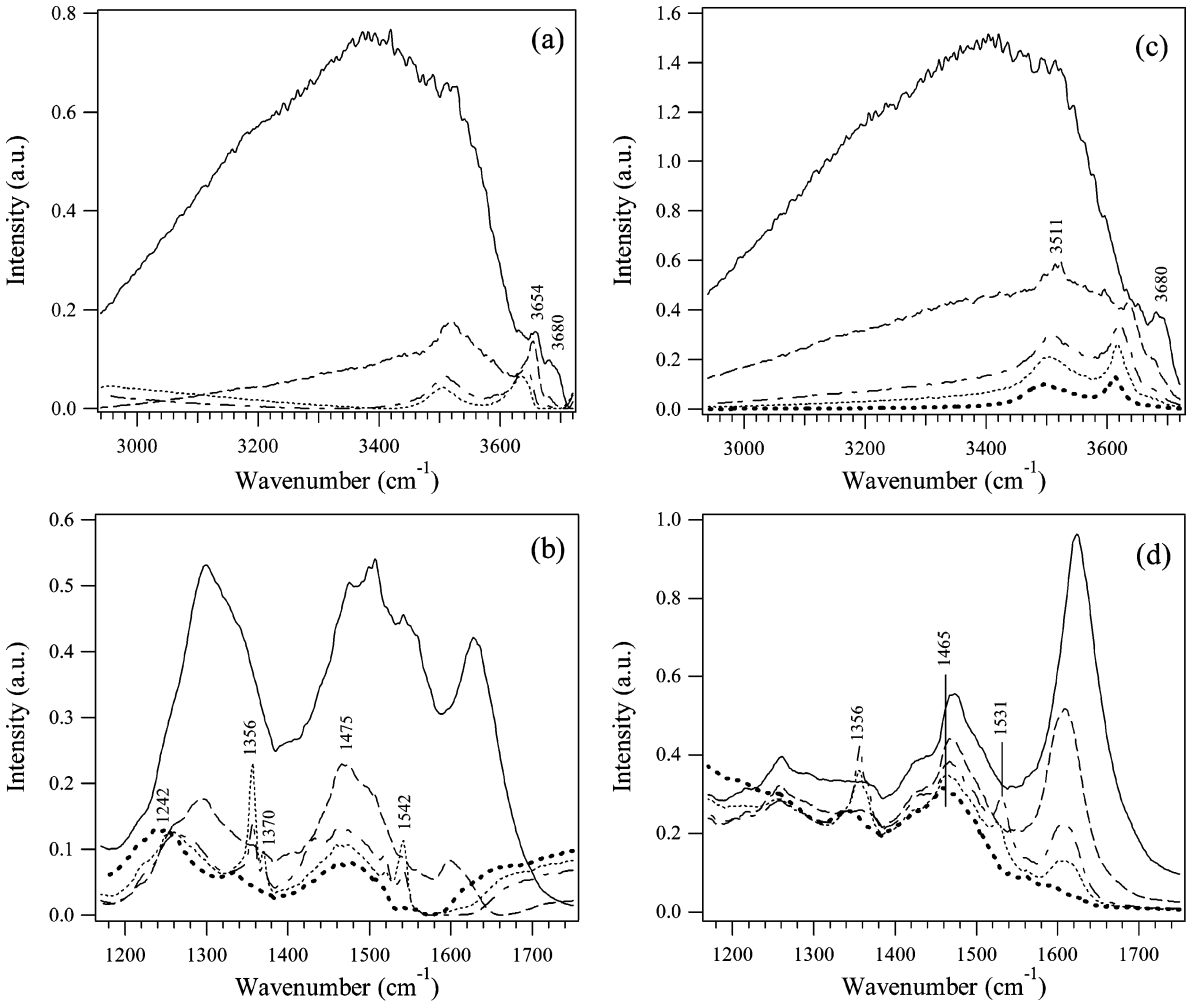

Figure 5. DRIFT spectra of the WO_3/CeO_2-supported oxides obtained at different temperatures: (—) room temperature, (- - -) 373, (- · - · -) 473, (· · ·) 523, and (• • •) 623 K. (a, b) Supported sample with $[W/Ce]_{nominal} = 0.025$. (c, d) Supported sample with $[W/Ce]_{nominal} = 0.070$. (a, c) Spectral region from 2940 to 3720 cm^{-1}. (b, d) Spectral region from 1150 to 1750 cm^{-1}.

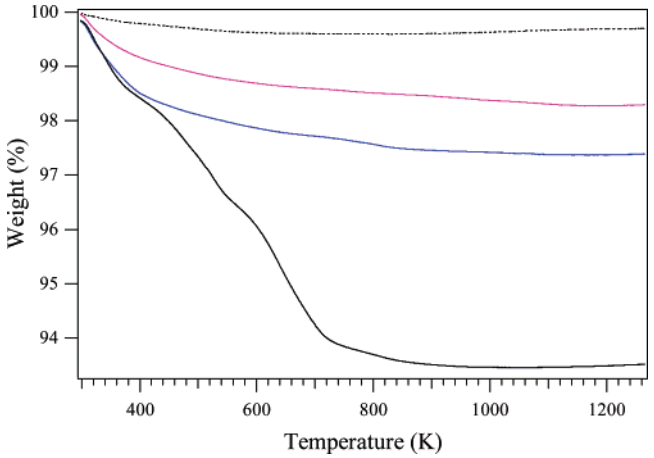

Figure 6. TG spectra (recorded in N_2) of (black line) CeO_2 treated at 523 K, (dotted line) WO_3 treated at 773 K, and the supported oxides with $[W/Ce]_{nominal}$ = (blue line) 0.025, (magenta line) 0.070.

1541 cm^{-1})[46] carbonate species as well as inorganic carboxylates (1506 cm^{-1}).[45−47] Narrow signals at 1356, 1370, 1520, and 1542 cm^{-1} are evident between 473 and 523 K, suggesting formation of new bidentate carbonate species and thus new active sites constituted by a Lewis acidic site (coordinatively unsaturated cation) with a coordinatively unsaturated neighboring oxygen anion. Formation of these species is favored by desorption of molecularly adsorbed water and by condensation of H-bound hydroxyl groups.

Only the contributions at 1242 and 1475 cm^{-1} are still observed at 623 K.

In the O−C−O spectral region of the supported oxide with $[W/Ce]_{nominal} = 0.070$, several contributions can be observed: 1427, 1472, 1260, and 1624 cm^{-1}. Heat treatment causes a large decrease of the signal at 1624 cm^{-1}, suggesting it is attributed to the hydroxyl bending of chemisorbed water and allows a new peak to be observed at about 1600 cm^{-1}. These data agree with the presence of mono- (1427 and 1472 cm^{-1}) and bidentate (1260 and 1600 cm^{-1}) carbonate species.

New peaks at 1356 and 1531 cm^{-1}, ascribable to bidentate carbonate species, appear at 473 and 523 K. At high temperature (573−623 K) the IR spectra only reveal monodentate carbonates (1465 cm^{-1}).

It is noteworthy that carbonates, very evident on the surface of ceria,[19] were never observed on the WO_3 surface.[31] Carbonate species are less evident in the nanocomposite oxides with respect to the supporting CeO_2[19] and decrease

(46) Li, C.; Sakata Y.; Arai, T.; Domen, K.; Maruya, K.-I.; Onishi, T. *J. Chem. Soc., Faraday Trans. 1* **1989**, *85*, 1451.
(47) Gatehouse, B. M.; Livingstone S. E.; Nyholm, R. S. *J. Chem. Soc.* **1958**, 3137.

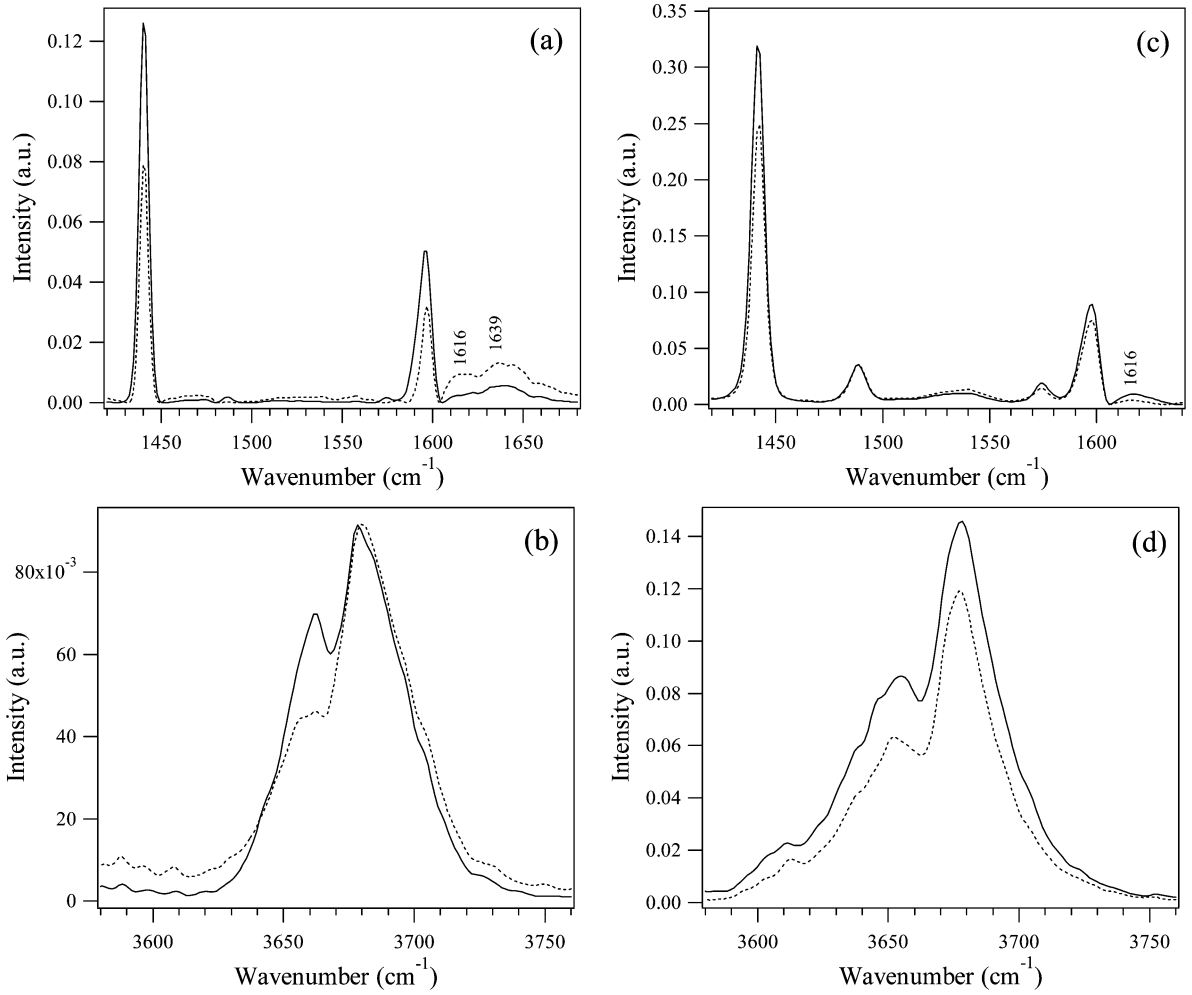

Figure 7. DRIFT spectra obtained after exposing the WO_3/CeO_2-supported oxides to pyridine (—) and successively to N_2 (···) at room temperature. (a, b) Supported sample with $[W/Ce]_{nominal} = 0.025$. (c, d) Supported sample with $[W/Ce]_{nominal} = 0.070$. (a, c) Pyridine stretching modes spectral region. (b, d) O−H stretching spectral region.

with heat treatments, thus suggesting a lower strength of the active sites responsible for the interaction with atmospheric carbon dioxide. Unfortunately the presence of carbonate species cannot be evidenced by XPS analysis because the Ce 4s peak is at the same position of the carbon in the carbonates.[29]

(b) Interaction with Pyridine. The DRIFT spectra obtained after exposure of the nanocomposite samples characterized by $[W/Ce]_{nominal} = 0.025$ and 0.070 to pyridine at room temperature are shown in Figure 7. Spectral inspection allows one to identify several contributions at 1440, 1486, 1575, 1596, and 1610−1640 cm^{-1} (Figure 7a,c). Comparison with literature data suggests the presence of pyridine H-bound to the surface hydroxyl groups (1440, 1486, 1575, 1596 cm^{-1});[48,49] the peaks at higher wavenumber, instead, are attributed to pyridine interacting with acidic sites. The shape of the signal over 1600 cm^{-1} differs significantly in the two nanocomposite oxides (Figure 7a,c). A peak at 1616 cm^{-1} in the spectrum of the supported sample with $[W/Ce]_{nominal} = 0.070$ (Figure 7c) is ascribable to pyridine interacting with Lewis acidic sites distributed on the surface.[48,49] Two contributions, respectively, at 1616 and 1639 cm^{-1}, are observed in the spectrum obtained after exposing the supported sample with $[W/Ce]_{nominal} = 0.025$ to pyridine (Figure 7a). The contribution at higher wavenumber suggests the presence of Lewis acidic sites of higher strength. By comparing the intensity of the spectra obtained for the two samples a higher amount of acidic sites in the nanopowder with $[W/Ce]_{nominal} = 0.070$ is evident. The sample with $[W/Ce]_{nominal} = 0.025$, in contrast, is characterized by a wide variety of acidic sites.

A broad band constituted by two components (around 3650 and 3678 cm^{-1}, Figure 7b,d) appears in the spectral region characteristic of O−H stretching vibrations as a consequence of exposure to pyridine and suggests perturbation of the hydroxyl groups. According to literature data[41] these contributions are attributed to hydroxyl groups bicoordinated to Ce(IV) cations (3650 cm^{-1}) and to Ce(IV) and Ce(III) cations (3678 cm^{-1}). Both the pyridine interacting by H-bond and pyridine species coordinated to Lewis acidic sites may account for the hydroxyl perturbation.

The nanocomposite samples show a different behavior under N_2 flow (Figure 7, dotted line). In the sample with $[W/Ce]_{nominal} = 0.025$, H-bound pyridine desorbs whereas

(48) Zaki, M. I.; Hasan M. A.; Al-Sagheer, F. A.; Pasupulety, L. *Colloids Surf. A* **2001**, *190*, 261.
(49) Zaki, M. I.; Hussein G. A. M.; Mansour, S. A. A.; El-Ammawy, H. A. *J. Mol. Catal.* **1989**, *51*, 209.

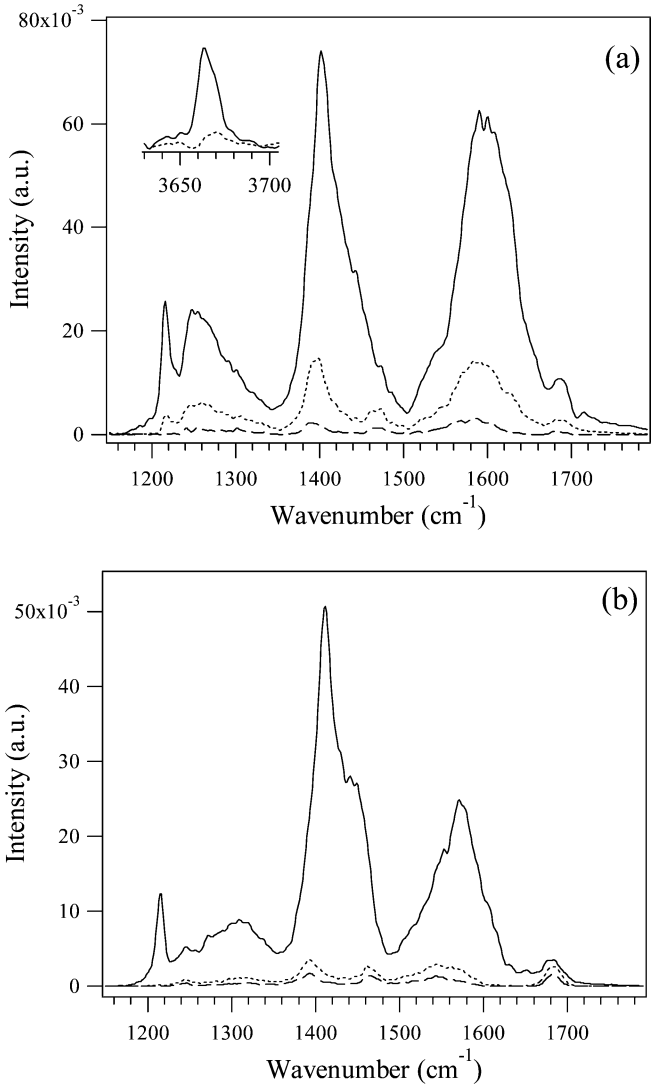

Figure 8. DRIFT spectra obtained at room temperature after exposing the WO_3/CeO_2-supported oxides characterized by $[W/Ce]_{nominal} = $ (a) 0.025 and (b) 0.070 to (—) CO_2 and successively to N_2 for (• • •) 2 and (- - -) 15 min. Spectral region from 1150 to 1790 cm^{-1}.

the pyridine interacting with the acidic sites increases, suggesting rearrangement of pyridine on the sample surface. The N_2 flow, in contrast, does not significantly remove pyridine from the surface of the sample richer in WO_3. Moreover, desorption of H-bound pyridine causes rearrangement of the hydroxyl groups, as evidenced in the O−H stretching region (Figure 7b,d).

Several acidic sites were observed on WO_3[20] (corresponding to the following IR peaks: 1608, 1614, 1625, 1643, and 1660 cm^{-1}), whereas on the supporting CeO_2 only contributions due to liquidlike pyridine and pyridine H-bound to the surface hydroxyl groups[19] were evidenced. Then, deposition of tungsten oxide favors formation of the acidic sites on the ceria surface. However, the acidic sites of the supported samples cannot be easily deduced from those of the pure oxides.

(c) Interaction with CO_2. At room temperature, CO_2 interacts with the surface of the WO_3/CeO_2 sample with $[W/Ce]_{nominal} = 0.025$, forming several carbonate species (Figure 8a): monodentate carbonate (1401 cm^{-1}), bidentate carbonate (1215, 1248, 1590 cm^{-1}) perturbed by the presence of tungsten oxide,[45,46] and bicarbonates[45,47] as suggested by the shoulder around 1680−1685 cm^{-1} and the contribution at 3664 cm^{-1} (see insert in Figure 8a).

The spectrum observed (Figure 8b) after exposing the sample with $[W/Ce]_{nominal} = 0.070$ to CO_2 at room temperature is similar to the one obtained for the sample with $[W/Ce]_{nominal} = 0.025$. The peaks at 1412 and at 1215, 1305, and 1570 cm^{-1} are due to mono- and bidentate species, respectively. The presence of bicarbonate species (1683 cm^{-1}) is also evident.

N_2 flow almost completely removes these species, indicating a very weak interaction of CO_2 with the nanocomposites surface; moreover, the shift toward lower wavenumber of the signals observed suggests a decrease of lateral interaction.[43]

It is worth remembering that carbon dioxide has never been observed to interact with WO_3.[20] Carbon dioxide does not interact with the supporting CeO_2 because the active sites distributed on the surface have already reacted with the atmospheric carbon dioxide, giving rise to different carbonate species.[19]

The above-mentioned results point out the presence, on the WO_3/CeO_2 sample surfaces, of new active sites with respect to supporting CeO_2; these can be described as basic active sites (giving rise to monodentate carbonate species) and complex sites constituted by a Lewis acidic site and a coordinatively unsaturated neighboring oxygen anion (originating bidentate carbonate species). Comparison of the intensity of the DRIFT spectra in the O−C−O spectral range after exposure to CO_2 suggests a higher amount of basic sites and complex sites on the sample with lower WO_3 amount.

(d) Interaction with CO. The DRIFT spectra obtained after exposure of the sample with $[W/Ce]_{nominal} = 0.025$ to carbon monoxide at temperatures ranging from room temperature to 573 K are displayed in Figure 9. In the DRIFT spectrum recorded after the exposure at room temperature only the presence of gas-phase carbon monoxide is evident (peaks around 2118 and 2171 cm^{-1}, Figure 9a).[50] Trace amounts of carbonate species can be observed upon exposure to CO at 423 K (Figure 9b). Comparison with literature data suggests the presence of bidentate (1303, 1557 cm^{-1})[46] and two different monodentate (1392 and 1464 cm^{-1})[45] carbonate species. These species are different from those observed after exposing the sample to CO_2. As temperature increases, the intensity of the O−C−O stretching contributions becomes more and more intense. At $T \geq 523$ K new contributions ascribable to bidentate carbonate species (around 1360 and 1574 cm^{-1}) appear and grow with temperature. Moreover, formation of inorganic carboxylate species is also evident (contribution around 1506 cm^{-1}). Inspection of Figure 9a indicates a significant formation of carbon dioxide at $T \geq 473$ K, as evidenced from the increment of the contributions due to carbon dioxide between 2280 and 2400 cm^{-1}.

Concerning the sample characterized by $[W/Ce]_{nominal} = 0.070$ (Figure 10), the only product derived from CO interaction is carbon dioxide. As on the sample with a lower

(50) Herzberg, G. *Infrared and Raman Spectra of Polyatomic Molecules*; Van Nostrand: New York, 1949.

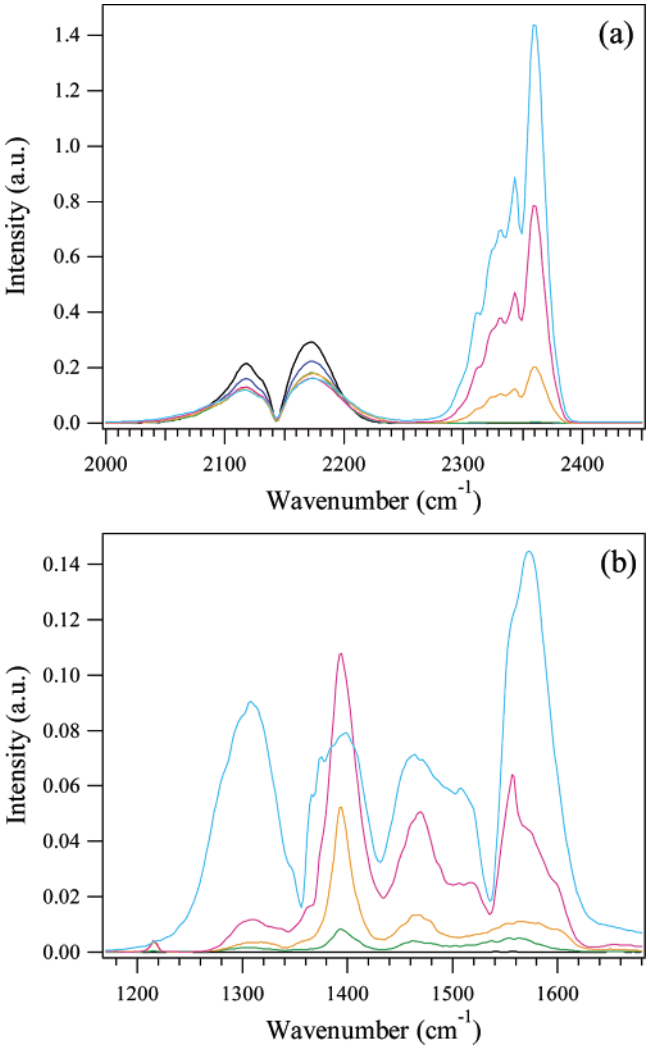

Figure 9. DRIFT spectra obtained after exposing the WO_3/CeO_2-supported oxide with $[W/Ce]_{nominal} = 0.025$ to CO at different temperatures: (black line) room temperature, (blue line) 373, (green line) 423, (yellow line) 473, (magenta line) 523, and (turquoise line) 573 K. (a) Spectral region from 2000 to 2450 cm^{-1}. (b) Spectral region from 1170 to 1680 cm^{-1}.

amount of WO_3, formation of carbon dioxide becomes important at $T \geq 473$ K. The absence of contributions characteristic of carbonate species suggests a negligible interaction between CO_2 and the surface active sites. This result agrees with the presence of a low amount of basic sites on this sample.

In Figure 11 the intensities of the CO and CO_2 DRIFT peaks are shown as a function of the exposure temperature. At a first glance it is evident that both the nanocomposite oxides catalyze the oxidation of CO to CO_2. However, inspection of the two CO_2 curve trends suggests that conversion of CO to CO_2 is more favorable at low temperature on the catalyst with lower WO_3 content but is more effective at high temperature ($T \geq 523$ K) on the sample with $[W/Ce]_{nominal} = 0.070$. The oxidation capability shown by both nanocomposite samples could be related to the different distribution of the Ce(III)/Ce(IV) and/or W(V)/W(VI) redox couples as evidenced by XPS analysis.

All reaction products weakly interact with the active sites distributed on the two WO_3/CeO_2-supported samples surfaces as demonstrated by the DRIFT spectra obtained after exposure to N_2; in fact, N_2 completely removes CO, CO_2, and carbonates from the surface.

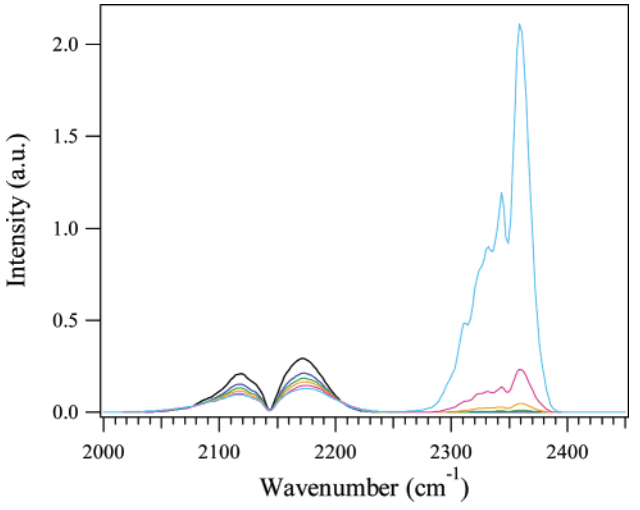

Figure 10. DRIFT spectra obtained after exposing the WO_3/CeO_2-supported oxide with $[W/Ce]_{nominal} = 0.070$ to CO at different temperatures: (black line) room temperature, (blue line) 373, (green line) 423, (yellow line) 473, (magenta line) 523, and (turquoise line) 573 K. Spectral region from 2000 to 2450 cm^{-1}.

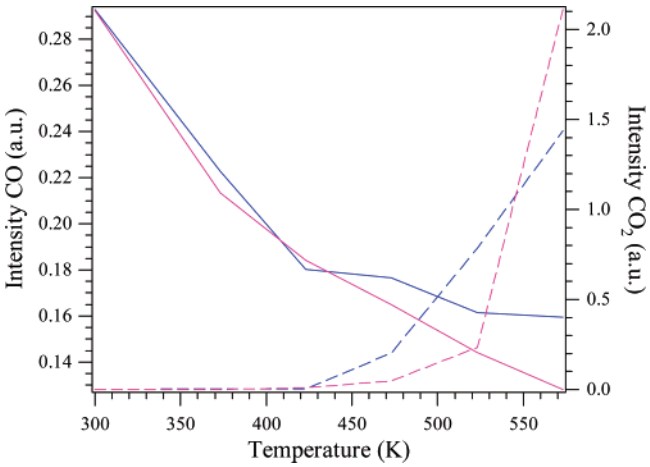

Figure 11. Intensities of the CO (solid line) and CO_2 (dashed line) DRIFT peaks displayed as a function of temperature: WO_3/CeO_2-supported oxides with $[W/Ce]_{nominal}$ = (blue line) 0.025 and (magenta line) 0.070.

It is worth noting that CO was observed to interact with WO_3, giving rise to a peak at about 2060 cm^{-1}.[20]

(e) Interaction with Methanol. The DRIFT spectra collected after exposure of the nanocomposite with $[W/Ce]_{nominal} = 0.025$ to methanol and successively to N_2 at temperatures ranging from room temperature to 573 K are shown in Figure 12. Several contributions are evident in the C−O stretching region (Figure 12a): 1038, 1048, 1060, and 1104 cm^{-1}. Comparison with literature data[19,51−55] suggests formation of methoxy species mono- (1104 cm^{-1}) and bicoordinated (1038, 1048, and 1060 cm^{-1}) to Ce(IV) cations. The presence of methoxy groups is confirmed by the signals corresponding to the symmetric and asymmetric C−H stretching observed at 2804, 2913, and 2922 cm^{-1} (Figure 12b).

(51) Badri, A.; Binet C.; Lavalley, J.-C. *J. Chem. Soc., Faraday Trans.* **1997**, *93*, 1159.
(52) Siokou, A.; Nix R. M. *J. Phys. Chem. B* **1999**, *103*, 6984.
(53) Binet, C.; Daturi M. *Catal. Today* **2001**, *70*, 155.
(54) Binet, C.; Jadi, A.; Lavalley, J.-C. *J. Chim. Phys.* **1992**, *89*, 1441.
(55) Daturi, M.; Binet, C.; Lavalley, J.-C.; Galtayries, A.; Sporken, R. *Phys. Chem. Chem. Phys.* **1999**, *1*, 5717.

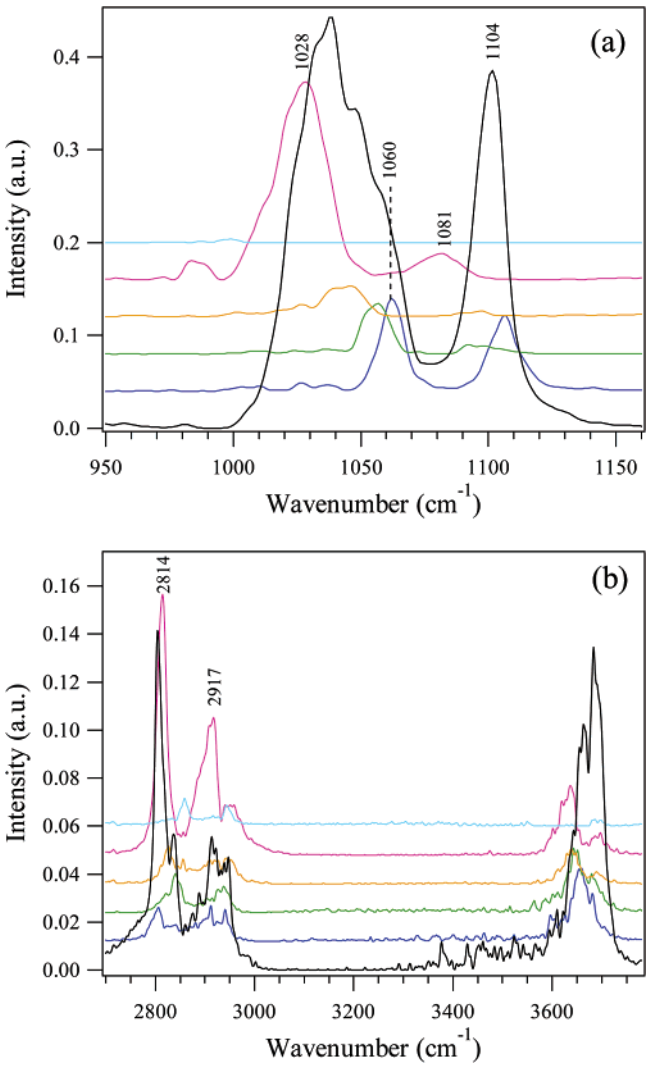

Figure 12. DRIFT spectra obtained after exposing the WO_3/CeO_2-supported oxide with $[W/Ce]_{nominal} = 0.025$ to methanol and successively to N_2 at different temperatures: (black line) room temperature, (blue line) 373, (green line) 423, (yellow line) 473, (magenta line) 523, and (turquoise line) 573 K. (a) Spectral region from 950 to 1160 cm^{-1}. (b) Spectral region from 2700 to 3780 cm^{-1}.

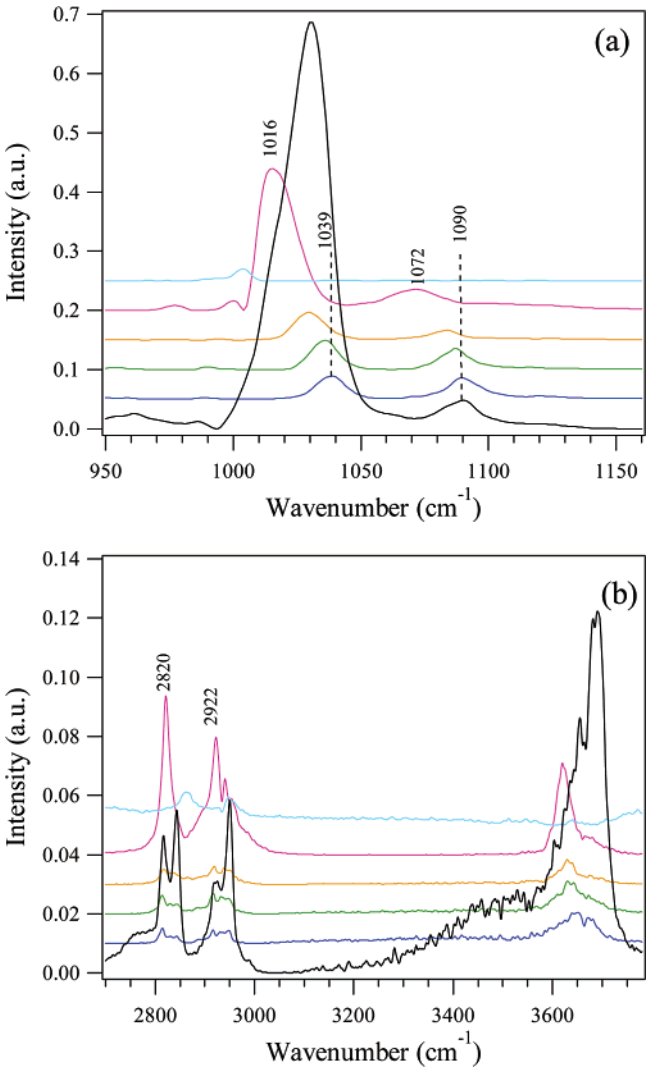

Figure 13. DRIFT spectra obtained after exposing the WO_3/CeO_2-supported oxide with $[W/Ce]_{nominal} = 0.070$ to methanol and successively to N_2 at different temperatures: (black line) room temperature, (blue line) 373, (green line) 423, (yellow line) 473, (magenta line) 523, and (turquoise line) 573 K. (a) Spectral region from 950 to 1160 cm^{-1}. (b) Spectral region from 2700 to 3780 cm^{-1}.

Methanol interacts mainly molecularly with the sample with $[W/Ce]_{nominal} = 0.070$,[50] as indicated by the peak centered at 1032 cm^{-1} and the corresponding symmetric and asymmetric C−H stretching contributions at 2845 and 2950 cm^{-1} (Figure 13). The difference in the methanol interaction mechanism agrees with the acidic/basic sites distribution discussed above. A weak and broad signal at 1090 cm^{-1} (Figure 13a) agrees with the presence of methoxy groups bicoordinated to Ce(III) ions[51,53] (see also C−H stretching contributions at 2817, 2918 cm^{-1}; Figure 13b). This contribution is similar to that observed after exposing a reduced CeO_2 sample to methanol.[19]

It is worth considering that at room temperature methanol interacts molecularly with WO_3[31] and both molecularly and dissociatively with ceria.[19]

On both samples several signals in the O−H stretching region (3655, 3664, and 3683 cm^{-1}) agree with a direct dissociation mechanism, which gives rise to hydroxyl and methoxy groups (Figures 12b and 13b). Formation of water, suggested by the broad band at 3200−3600 cm^{-1} and the corresponding hydroxyl bending peak at 1625 cm^{-1}, can be a consequence of condensation between methanol and hydroxyl groups. This mechanism is more evident on the sample with $[W/Ce]_{nominal} = 0.070$ (Figure 13b).

Methanol dissociation is favored by the temperature increment: the contribution due to molecular chemisorbed methanol is no longer revealed. Two signals attributed to the C−O stretching vibration of methoxy groups can be revealed after exposure of the sample with $[W/Ce]_{nominal} = 0.025$ to methanol and successively to N_2 at $T \geq 373$ K; their positions agree with that of bi- (1060 cm^{-1}) and monocoordinated (1107 cm^{-1}) methoxy groups. In the sample with $[W/Ce]_{nominal} = 0.070$, besides the contribution due to methoxy groups bicoordinated to Ce(III) (1090 cm^{-1}), a new peak characteristic of methoxy groups bicoordinated to Ce(IV) is evident at 1039 cm^{-1}. As temperature increases, all signals shift toward lower wavenumber, suggesting a decrease of lateral interaction. Moreover, at high temperature direct dissociation is favored.

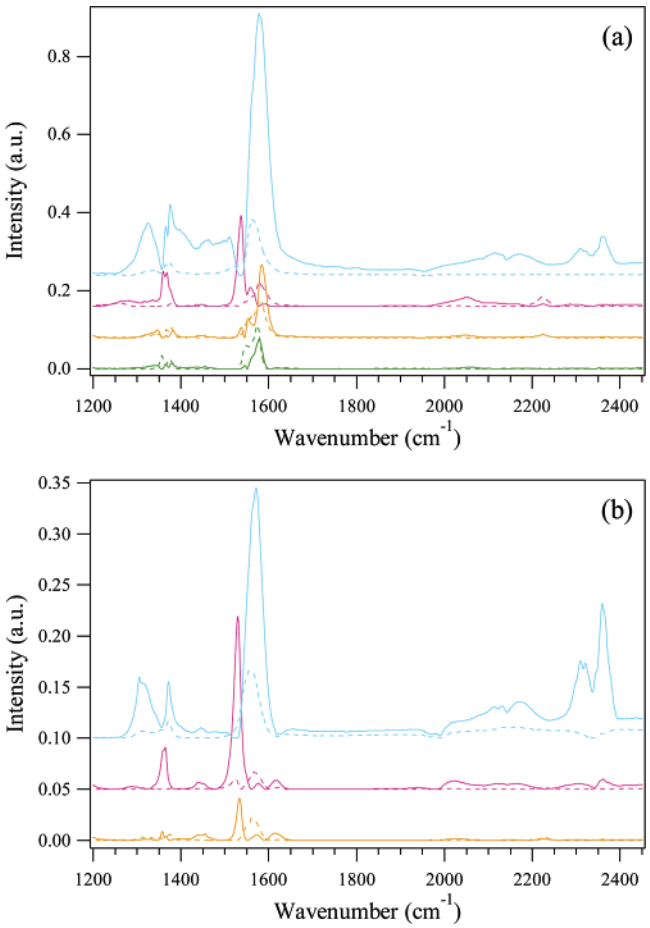

Figure 14. DRIFT spectra obtained after exposing the WO_3/CeO_2-supported oxides to methanol (solid line) and successively to N_2 (dotted line) at different temperatures: (green line) 423, (yellow line) 473, (magenta line) 523, and (turquoise line) 573 K. (a) Supported sample with $[W/Ce]_{nominal} = 0.025$. (b) Supported sample with $[W/Ce]_{nominal} = 0.070$. Spectral region from 1200 to 2450 cm^{-1}.

At 523 K new signals can be observed, after exposure to methanol and successively to N_2, at about 1028, 1081, 2814, and 2917 cm^{-1} for the sample with $[W/Ce]_{nominal} = 0.025$ and at 1016, 1072, 2820, and 2922 cm^{-1} for the sample with $[W/Ce]_{nominal} = 0.070$. These new signals agree with formation of methoxy species different from those observed at lower temperatures. In particular, the peaks at lower wavenumber in the C−O stretching region (1028 and 1016 cm^{-1}) are consistent with the formation of tricoordinated methoxy groups.

The temperature increment also favors methanol oxidation on both samples. In the nanocomposite with $[W/Ce]_{nominal} = 0.025$ several peaks attributed to bidentate formate species[31,52,56] (1356, 1373, 1547, and 1578 cm^{-1}) are evident at 423 K (Figure 14a, solid line). At 473 K new contributions at 1368 and 1538 cm^{-1} indicate formation of new formate species. In the sample richer in WO_3 bidentate formate species (1355, 1371, and 1558 cm^{-1}) appear at 473 K and grow with temperature (Figure 14b, solid line). In both cases, product desorption is easier at higher temperatures (Figure 14, dotted line).

Formation of carbon monoxide and carbon dioxide at 573 K is suggested, on both the samples, by several signals at 2120, 2170, 2310, 2321, and 2359 cm^{-1}.

Comparison of the obtained spectra suggests that methanol dissociation is favored on the sample with $[W/Ce]_{nominal} = 0.025$. Moreover, on this sample methanol oxidation begins at lower temperature with respect to the sample with $[W/Ce]_{nominal} = 0.070$. In this last sample, however, higher selectivity toward formation of carbon dioxide is observed.

It is worth noting that both samples show a higher reactivity toward methanol oxidation than ceria.[19]

Conclusions

Several WO_3/CeO_2 nanocomposite powders, differing in W/Ce atomic ratio ($[W/Ce]_{nominal} = 0.010$, 0.025, 0.040, 0.055, 0.070, 0.085), were synthesized by wet impregnation and characterized by means of XRD, TGA, XP, and DRIFT spectroscopic techniques as well as TEM and EDS.

XRD data are consistent with the presence of cubic CeO_2, whereas contributions due to WO_3 were never observed. The average diameter of the WO_3/CeO_2 particles is around 13 nm. TEM and EDS results suggest a homogeneous distribution of WO_3 on the CeO_2 surface.

XP outcomes allow us to identify the presence of Ce(III) and W(V) at the interface between WO_3 and CeO_2.

DRIFT analysis reveals that carbonate species are evident on the nanocomposite oxides surface but to a lower extent than on the surface of cerium oxide.

The active sites distributed on the surface of the two samples were also investigated by studying the interaction with probe molecules (pyridine, CO, and CO_2). Interaction with pyridine emphasizes the presence of different Lewis acidic sites on the surface of the nanocomposite oxide characterized by $[W/Ce]_{nominal} = 0.025$ and of only one Lewis acidic site on the surface of the sample richer in WO_3. Exposure to CO_2 allows us to recognize the presence of basic sites and complex sites constituted by a Lewis acidic site and a coordinatively unsaturated neighboring oxygen anion. Basic and complex sites become less evident with increasing W/Ce atomic ratio.

Both WO_3/CeO_2 nanocomposites oxidize CO to CO_2 at $T > 423$ K, but the sample richer in WO_3 shows a higher oxidation capability.

Methanol interacts both molecularly and dissociatively with the WO_3/CeO_2 samples; dissociation is prevalent on the sample characterized by $[W/Ce]_{nominal} = 0.025$, whereas a mainly molecular interaction is observed on the sample with $[W/Ce]_{nominal} = 0.070$. Oxidation of methanol is evident on both samples: the sample with a lower amount of WO_3 is more active at rather low temperatures, whereas the sample richer in WO_3 shows a higher selectivity with respect to formation of carbon dioxide.

Acknowledgment. The authors gratefully acknowledge Professor E. Tondello for his helpful discussions, Dr. R. Saini for thermal analysis, and Padova University for financial support. This work was supported by the research program FISR-MIUR "Nanosistemi inorganici ed ibridi per lo sviluppo e l'innovazione di celle a combustibile".

(56) Li, C.; Domen, K.; Maruya, K.; Onishi, T. *J. Catal*. **1990**, *125*, 445.

CM0603654